MODELLING OF FRACTIONAL CRYSTALLIZATION OF BASALTS ALONG THE GALAPÁGOS SPREADING CENTER

Research Thesis

Submitted in partial fulfillment of the requirements for graduation
with research distinction in Earth Sciences in the undergraduate colleges
of The Ohio State University

By

Nurnadira Sazali
The Ohio State University
2018

Approved by

Dr. Michael Barton, Advisor
School of Earth Sciences

TABLE OF CONTENTS

Abstract……....ii

Acknowledgements……..iii

List of Figures……..iv

List of Tables……....v

Introduction……..1

Geologic Setting……..2

Methods……...4

Results……6

Discussion……...16

Conclusions……..20

Recommendations for Future Work……21

References Cited…….22

Appendix……25

ABSTRACT

The Galápagos Spreading Center (GSC) lies at the boundary of two tectonic plates, the Nazca Plate and the Cocos Plate in the eastern equatorial Pacific with an intermediate spreading rate. The GSC provides an insight to the plume-ridge interaction as it lies north of the Galápagos Islands Archipelago with the mantle plume located at 91°W. Processes that relate to the plume-ridge interaction and geochemical variations that affect the compositions of oceanic crust and evolutionary processes can be determined by modelling the fractional crystallization of mid-ocean ridge basalts (MORB) along the GSC. The PETROLOG program was used to model the crystallization of MORB by using the published dataset of natural glasses. The crystallization models of parental magmas were then compared with the compositional data of the natural glasses for each segment on the GSC to find the best fit of calculated crystallization lines. The results reveal that the crystallization of olivine, plagioclase, clinopyroxene, ilmenite, and magnetite at a low pressure best explains the compositions of the natural glasses along the GSC. The amount of water content and oxygen fugacity play an important role in the crystallization pathway of MORB. The behavior of the major oxides suggests that fractional crystallization together with crustal assimilation and mixing have occurred along the GSC that affected the compositions of MORB.

ACKNOWLEDGEMENTS

I would like to express the deepest appreciation to my research advisor, Dr. Michael Barton for providing me the opportunity to conduct this research and the guidance to work on this research. I would also like to express my gratitude to Ministry of Rural Development Malaysia Federal Agency, Majlis Amanah Rakyat (MARA) for funding my bachelor's degree at The Ohio State University. Moreover, I would like to thank Dr. Barton's graduate students, Katherine Haines and Ken Peterman for their great wealth of knowledge and recommendations. Katherine has been a great influence on me and she provided valuable insight and expertise that greatly helped my research. I would also like to thank Dr. Anne Carey for her patience and advice during my research experience and Ariff Amin for his helpful advice on my thesis. In addition, I am thankful to my best friend, Anis Hishammudin for encouraging and supporting me throughout the time of my research. Finally, a personal thank you to all my family and friends for always believing in me and pushing me to be the best person I could be. Without them, this thesis would not have been possible.

List of Figures

1. Map of studied region
2. Map of studied region divided into 10 segments
3. Graphs of P_2O_5 vs. K_2O at segments E, F, and H
4. Graphs of major oxides vs. MgO with no added H_2O at segment E
5. Graphs of major oxides vs. MgO with 0.1% added H_2O at segment E
6. Graphs of major oxides vs. MgO for lower MgO parent (0.2% added H_2O) at segment F
7. Graphs of major oxides vs. MgO for higher MgO parent (0.2% added H_2O) at segment F
8. Graphs of major oxides vs. MgO with $fO_2 = 0$ at segment H
9. Graphs of major oxides vs. MgO with $fO_2 = +1$ at segment H
10. Graphs of Al_2O_3 and FeO vs MgO, Peterson *et al*. (2014)

A1. Graphs of major oxides vs. MgO with $fO_2 = +1$ and 0.1% added H_2O at segment E

B1. Graphs of major oxides vs. MgO with $fO_2 = +1$ and 0.2% added H_2O at segment F

C1. Graphs of major oxides vs. MgO with $fO_2 = +1$ and 0.1% added H_2O at segment H

D1. Na_8 vs. longitude at segments E, F, and H

D2. Fe_8 vs. longitude at segments E, F, and H

D3. Ti_8 vs. longitude at segments E, F, and H

D4. Si_8 vs. longitude at segments E, F, and H

LIST OF TABLES

1. Pressures of crystallization at all segments, Haines (2016)

INTRODUCTION

The mid-ocean ridge is the largest mountain chain and the most active system of volcanoes in the solar system (Macdonald, 2001). The ridge, which is approximately 70,000 km long and ~5-30 km wide, is located between plates of the Earth's rigid outer shell that are separating at speeds of ~10-170 mm/yr (Macdonald, 2001) and is producing 75% of Earth's volcanism (Crisp, 1984), thus creating two thirds of Earth's crustal area (Gale *et al.,* 2013). The existence of mantle plumes is thought to cause the mid-ocean ridge system to have physical and chemical anomalies (Cushman *et al.,* 2004). Variations in spreading rate along the global mid-ocean ridge system are accompanied by the variations in crustal structure (Colman *et al*., 2016) and the variations in magma supply (Colman *et al.,* 2016). The Galápagos Spreading Center (GSC) is focused in this research thesis for its intermediate spreading rate and its off-axis plume that strongly influences the ridge, which is useful for studying the plume-ridge interaction.

Basalts, which are the product of melting of the mantle, migration of melt through the mantle towards the surface, and cooling and differentiation of magma near the surface form the upper portion of the ocean crust (Langmuir *et al.*, 1992), are used to infer magma generation conditions in the mantle (Niu and Batiza, 1994; Langmuir *et al.,* 1992; Danyushevsky, 2001) and understand the processes that had happened during the formation of basalts. The modelling of the evolution of magmas at the mid-ocean ridge can determine the processes that result in the geochemical variations in basalts.

The purpose of this research thesis is to model the evolution of mid-ocean ridge basalts (MORB) along the GSC and estimate the pressures in which the magmas partially crystallize. This was done by calculating the crystallizations of olivine, plagioclase, clinopyroxene, ilmenite, and magnetite that form in basalts. The compositions of these magmas were also analyzed in detail to examine the processes that have occurred during the magma evolution along the GSC. Previous work done by O'Hara (1977, 1985) suggests that most basalts lie on low-pressure cotectic; therefore, this study can test the hypothesis of the MORB crystallizing at low pressures and provide information on the depths in which these mid-ocean ridges magmas partially crystallize and the geochemical variations in MORB along the GSC.

GEOLOGIC SETTING

The Galápagos Spreading Center (GSC) is a mid-ocean ridge that forms the divergent plate boundary between the two tectonic plates: the Cocos and Nazca Plates (Canales *et al*., 2014) at an intermediate full spreading rate of approximately 46 to 64 mm/yr (Kokfelt et al., 2005). The GSC, also known as the Cocos-Nazca Spreading Center, is strongly influenced by the presence of the Galápagos hotspot in terms of its structure, morphology, and compositions (Kokfelt et al., 2005). The Galápagos hotspot is located near 91.5°W and produced two aseismic ridges, the Cocos and Carnegie Ridges (Merlen, 2014) at approximately 22 Ma and 20 Ma ago (Merlen, 2014). The Cocos Ridge lies on the Cocos Plate to the north and is moving to the northeast while the Carnegie Ridge lies on the Nazca Plate to the south and is moving to the east (Merlen, 2014). The Galápagos Islands are a hotspot-related chain that lies approximately 200 km south of the ridge (Cushman et al., 2004). The GSC is offset about 100 km by a transform fault located at 91°W (Kokfelt et al., 2005) and has been progressively drifting northwards over the past 5 Ma (Herbrich et al., 2016). The Galápagos Islands, the Cocos and Carnegie Ridges demonstrate the activity and evolution of the Galápagos hotspot and its interaction with the GSC (Canales *et al.,* 2002).

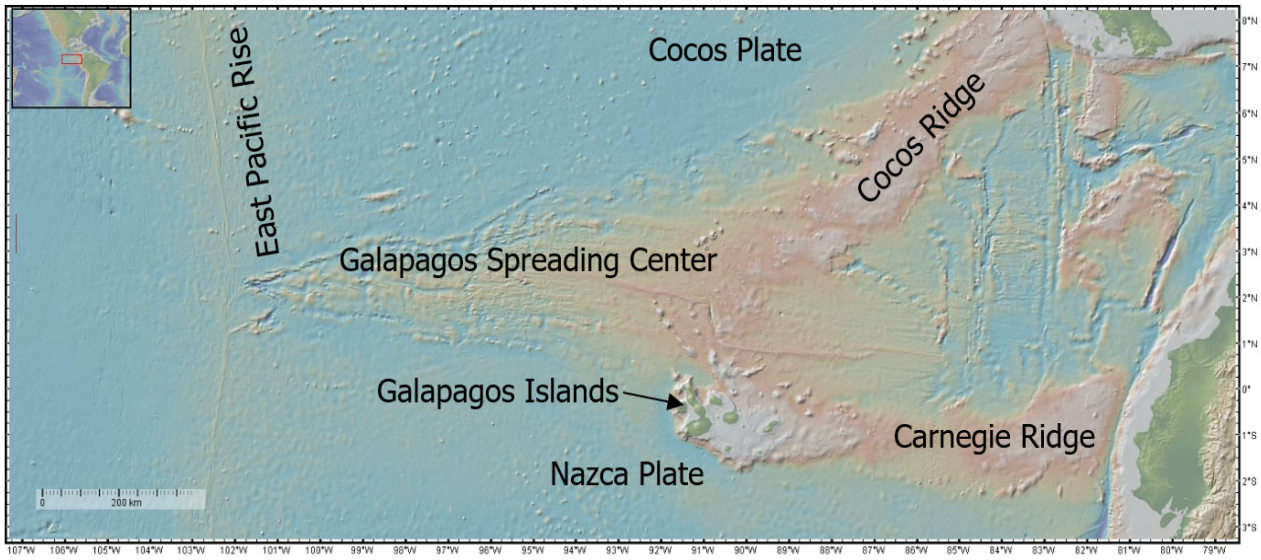

Figure 1: A map showing the region of study on the Galápagos Spreading Center (GSC) and the location of the nearby Galápagos Islands in the East Pacific Ocean. The map also shows the location of the Carnegie Ridge on the Nazca Plate and the location of the Cocos Ridge on the Cocos Plate as well as the location of the East Pacific Rise. The Galápagos hotspot is located beneath the Nazca Plate. The map was generated using the software *GeoMapApp*.

The average rate of magma supply, the thickness of the ridge, and the axial depths are all affected with proximity to the hotspot (Colman *et al.,* 2016). With greater proximity to the hotspot, the average rate of magma supply to the crust is increased, the crust will be thicker, and the axial depths will be shallower (Colman *et al.,* 2016). The crustal thickness along the GSC increases from ~5.7 km at 97°W to ~7.9 km at 91.5°W (Canales *et al.,* 2002). The GSC also has an axial high morphology within ~350 km of the Galápagos hotspot in which it changes to a

transitional morphology away from the hotspot (Cushman et al., 2004). Therefore, the GSC provides a good setting for studying the plume-ridge interaction and understanding the processes that are affected by this interaction.

METHODS

Sampling methodology

Data were obtained online from PetDB Database (www.earthchem.org/petdb) and 1,777 rock samples data were downloaded and compiled using Microsoft Excel. These samples consist of mid-ocean ridge basalts (MORB) that were collected from the ocean floor within the area of latitude 0.46°N to 3.2°N and longitude 101.75°W to 83.04°W along the Galápagos Spreading Center (GSC). The major oxides data included in the samples analysis were utilized in this research project to study the geochemical processes that took place during the crystallization of MORB.

All 1,777 rock samples were plotted in a desktop application called GeoMapApp according to their own locality. The samples were then divided into 10 different segments according to the amount of offset on the ridge, which were named alphabetically from A to J (Figure 2). Only three segments were chosen and examined closely for this thesis, which are segments E, F, and H. Segment E is the most heavily-sampled among the three studied segments with 577 glass analysis, Segment F consists of 188 glass analysis, and Segment H comprises 322 glass analysis.

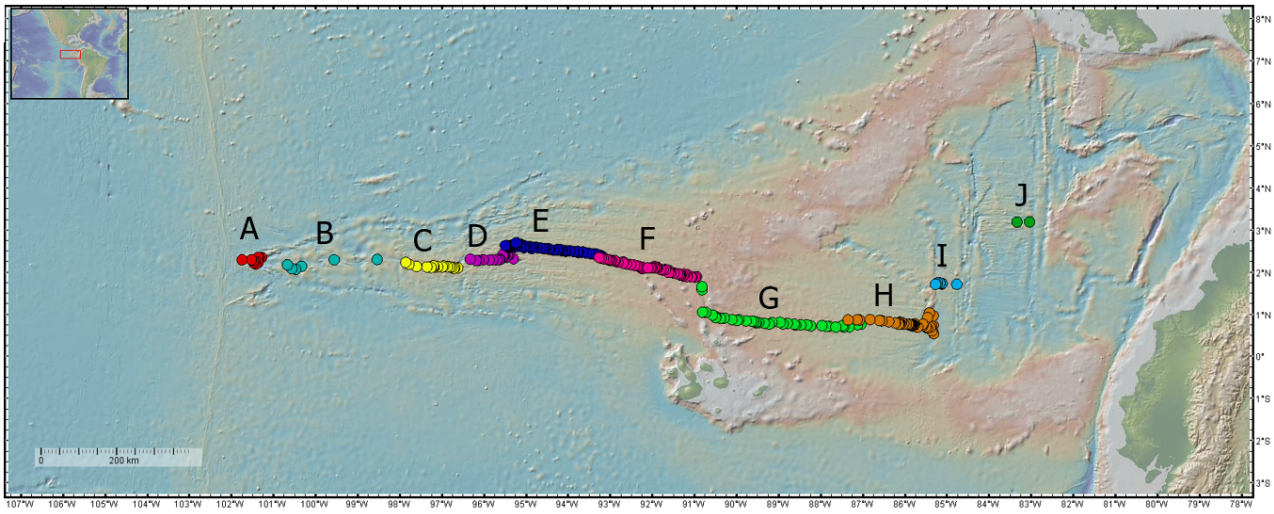

Figure 2: A map showing the rock samples plotted in different colors according to their segments along the Galápagos Spreading Center (GSC). The map was generated using the software *GeoMapApp*.

Modelling methodology

PETROLOG, a computer software program was used to model the crystallization process of the major oxides that make up the minerals present in MORB. PETROLOG incorporates 46 mineral-melt equilibrium models for 8 different minerals that enables the estimated crystallization pressure at which the melt composition is saturated with both olivine and clinopyroxene to be generated (Danyushevsky and Plechov, 2011). In order to produce the crystallization path in PETROLOG, a parental magma was first chosen for each segment based on the estimated crystallization pressure.

The major oxides in the parental magma were then normalized to 100% weight. The model Danyushevsky (2001) was selected for the minerals olivine, plagioclase, and clinopyroxene, while the model Ariskin and Barmina (1999) was selected for the minerals ilmenite and magnetite in the calculations.

The results of the calculations on PETROLOG were plotted using the software CoPlot to observe the chemical variations and to interpret the patterns of crystallization. This was done by plotting the oxides of elements SiO_2, Al_2O_3, TiO_2, FeO, CaO, and Na_2O - against MgO in weight percent values. MgO was chosen to be plotted against because MgO is compatible in olivine found in MORB and its amount decreases considerably as these basalts cool and crystallize (Langmuir et al., 1992). Most elements also vary regularly with MgO (Gale *et al.,* 2014). The FeO reported represents the FeO_{TOTAL} in which $FeO_{TOTAL} = 0.8998 * Fe_2O_3 + FeO$.

Segment E. 93.2°W – 95.5°W

KAK1979-012-026 (PetDB Database) was selected as the parental magma and its oxides elements were first normalized to 100% wt before its data were added to PETROLOG. The mineral-melt models chosen were Danyushevsky (2001) for minerals olivine, plagioclase, and clinopyroxene and Ariskin and Barmina (1999) for minerals ilmenite and magnetite. Calculations were done along a Quartz-Fayalite-Magnetite (QFM) buffer of oxygen fugacity. The model Kress and Carmichael (1988) was used for the melt oxidation state; Lange and Carmichael (1987*)* for melt density; and Giordano and Dingwell (2003*)* for viscosity. Three different pressures of crystallization were also set into the calculations: 0.5 kbar, 3 kbar, and 5 kbar to compare the effects of various pressures on the paths of crystallization. The calculations were then specified to stop at 75% of fractionation.

The calculations were repeated by shifting the QFM buffer by +1 log units, while also keeping the other parameters the same to test if better calculated crystallization trends were produced. The calculations were also done with three different amount of water content in the parental magma composition (0.1%, 0.2%, and 0.5%) to observe the effect of differing the melt water content on the composition of crystallizing minerals (Danyushevsky and Plechov, 2011).

Segment F. 90.95°W - 93.3°W

This segment is particularly interesting since the Galápagos hotspot is located near 91̊ 30’ W. The parental magma selected for this segment was EWI0004-015-004 (Cushman et al., 2004). All PETROLOG parameters and mineral-melt models chosen remained the same as for segment E. However, another parental magma, EWI0004-040-004 (Cushman et al., 2004) was also selected to examine the effect on having different parental magma compositions to the crystallization paths on the area near the hotspot.

Segment H. 85.3°W - 87.4°W

The parental magma that was selected was ALV1659-001 (PetDB Database). All PETROLOG parameters and mineral-melt models chosen remained the same as for segment E.

RESULTS

Figure 3 shows the plots of P_2O_5 against K_2O in wt% for the three segments: E, F, and H. Segments E and F exhibit similar results where the melt is more enriched in K_2O than P_2O_5 as crystallization proceeds. As for segment H, the melt is more enriched in P_2O_5 compared to K_2O during the initial crystallization, but it becomes more enriched in K_2O than P_2O_5 as crystallization proceeds.

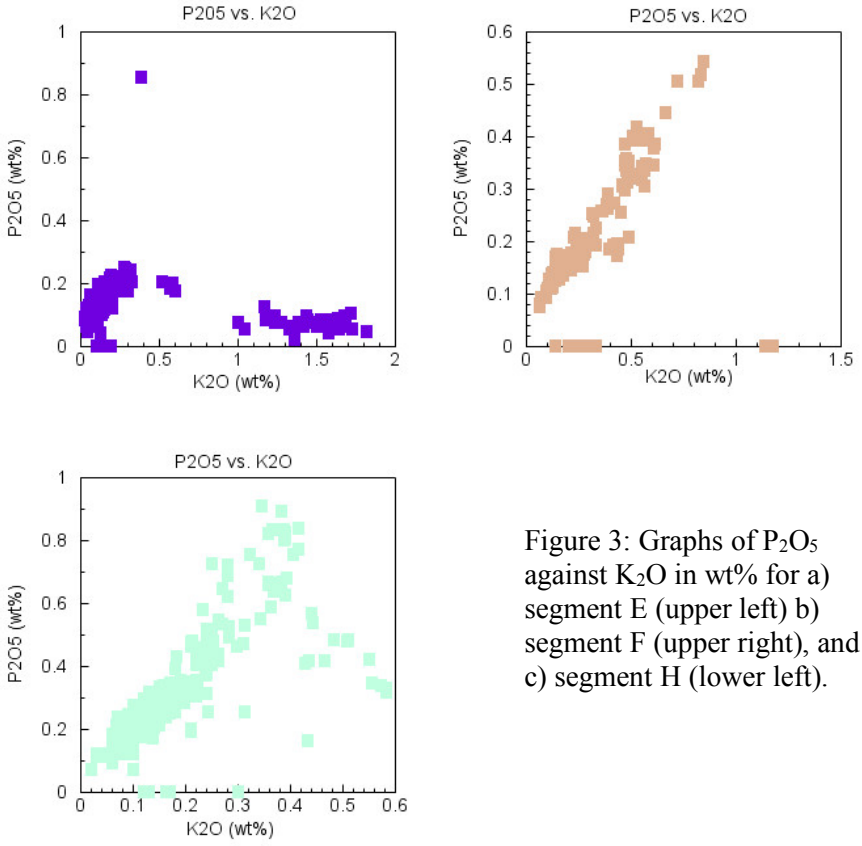

Figure 3: Graphs of P_2O_5 against K_2O in wt% for a) segment E (upper left) b) segment F (upper right), and c) segment H (lower left).

Segment E. 93.2°W – 95.5°W

Figure 4 and Figure 5 show the crystallization trend of the parental magma KAK1979-012-026 (PetDB Database) on segment E along the GSC. This parental magma produces better compositional results with 0.1% water added to the initial melt compared to no added water as the results with 0.1% water show a much closer agreement with the samples. The addition of water to the composition of parental magma results in the appearance of kinks in the trend lines of most oxides, which fit better with the compositions of the natural glasses (Figure 5). The results suggest that crystallization at a low pressure, 0.5 kbar, yields the best fit at this locality.

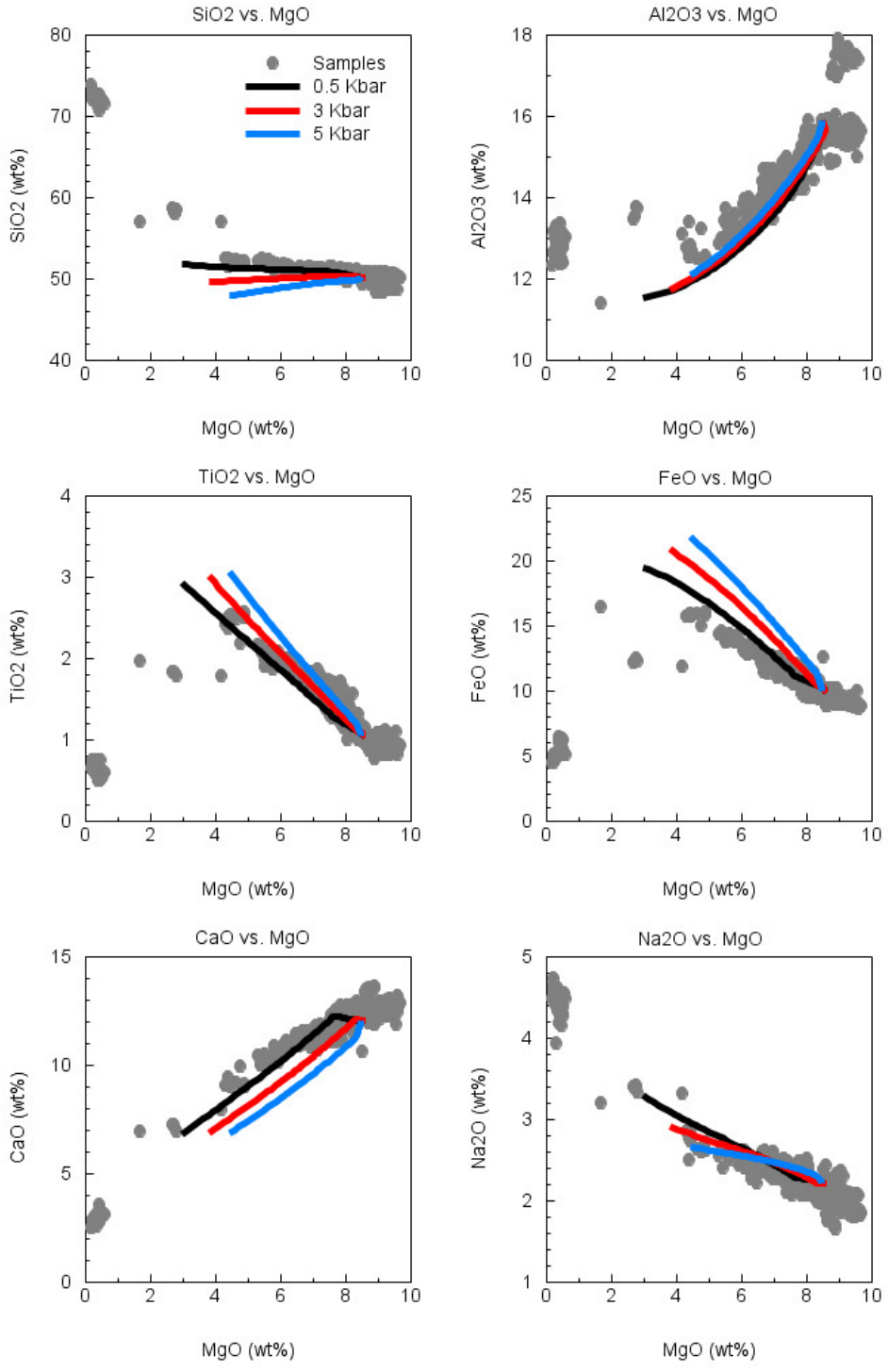

Figure 4: Graphs showing the weight % of the major oxides plotted against MgO for the parental magma KAK1979-012-026 (PetDB Database) on segment E along the GSC. The calculations were done using PETROLOG at various pressures (0.5 kbar, 3 kbar, and 5 kbar) with no water added to the initial melt.

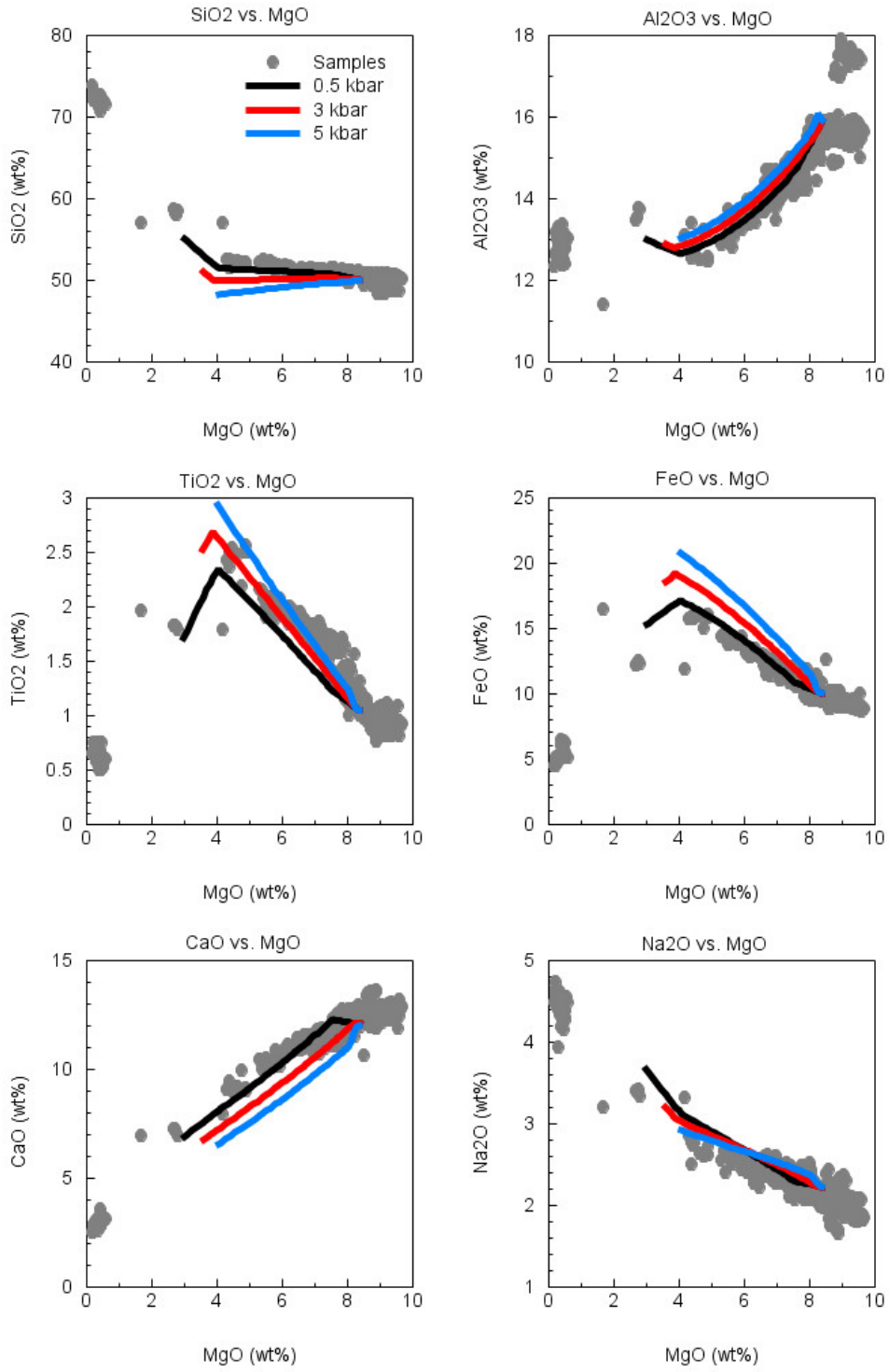

Figure 5: Graphs showing the weight % of the major oxides plotted against MgO for the parental magma KAK1979-012-026 (PetDB Database) on segment E along the GSC. The calculations were done using PETROLOG at various pressures (0.5 kbar, 3 kbar, and 5 kbar) with 0.1% water added to the initial melt.

Segment F. 90.95°W - 93.3°W

The crystallization results for two parental magma with different starting MgO compositions are presented in Figure 6 and Figure 7. The calculated liquid compositions for the lower MgO parent EWI0004-015-004 (Cushman et al., 2004) fit better with the data of the samples taken compared to the parent with a higher MgO content EWI0004-040-004 (Cushman et al., 2004). Once again, the results suggest that crystallization at a low pressure, 0.5 kbar, yields the best fit at this locality. However, there is an exception for TiO_2, in which the crystallization at higher pressures, 3 to 5 kbar, produces better fit lines than at lower pressure.

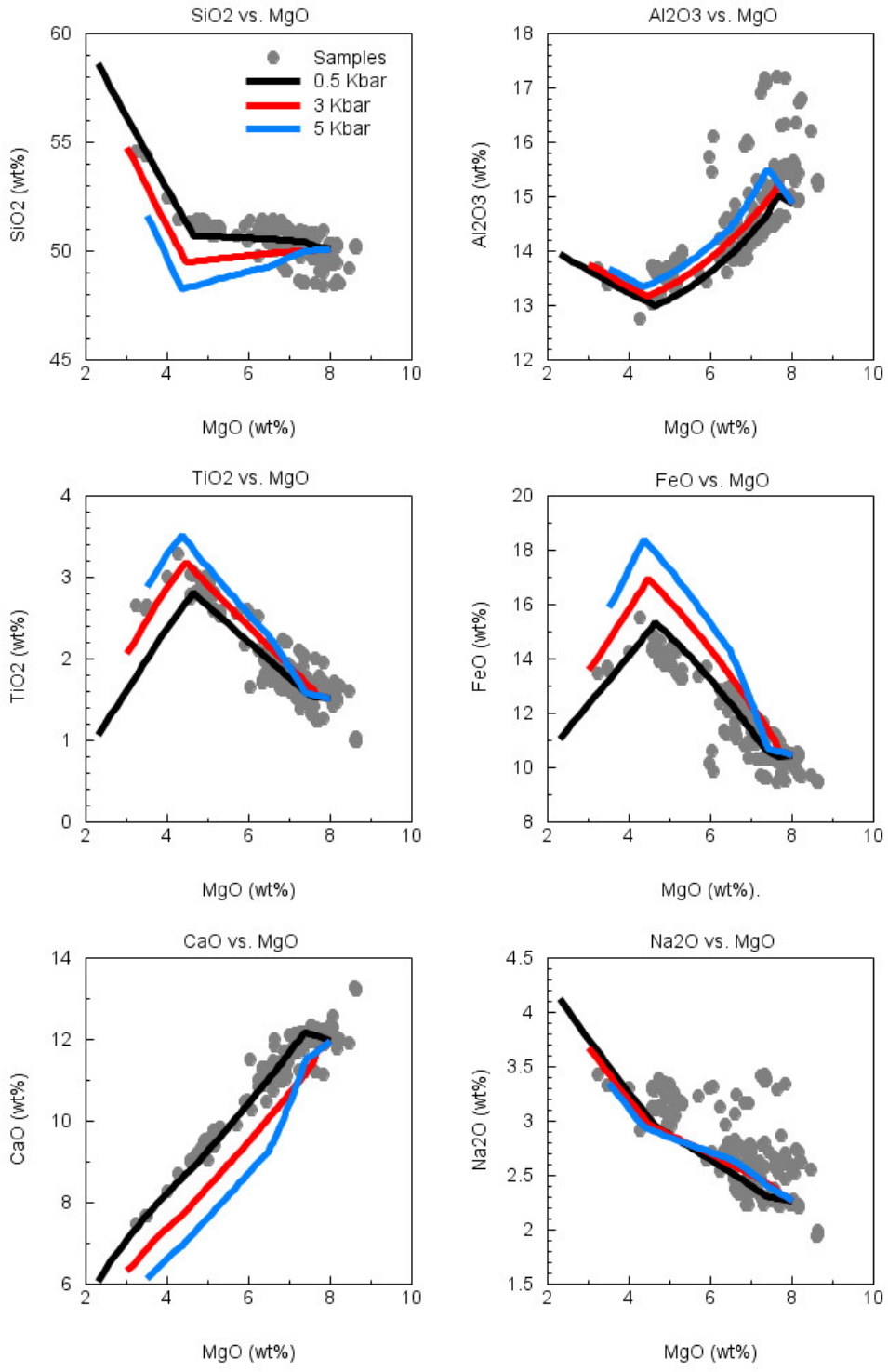

Figure 6: Graphs showing the weight % of the major oxides plotted against MgO for the parental magma EWI0004-015-004 (Cushman, 2004) on segment F along the GSC. The calculations were done using PETROLOG at various pressures (0.5 kbar, 3 kbar, and 5 kbar) with 0.2% water added to the initial melt.

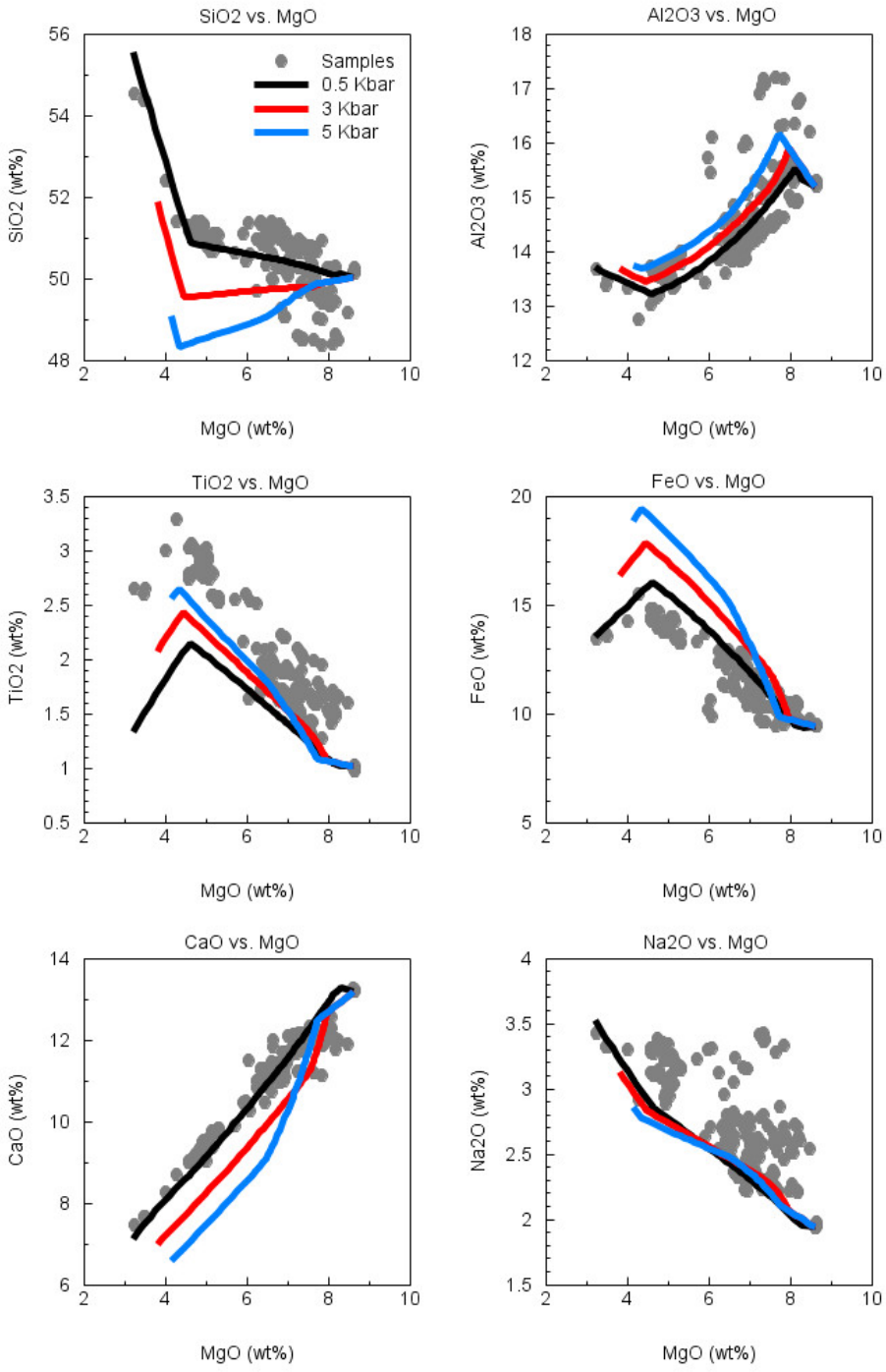

Figure 7: Graphs showing the weight % of the major oxides plotted against MgO for another parental magma EWI0004-040-004 (Cushman, 2004) on segment F along the GSC. The calculations were done using PETROLOG at various pressures (0.5 kbar, 3 kbar, and 5 kbar) with 0.2% water added to the initial melt.

Segment H. 85.3°W - 87.4°W

The calculated liquids lines for the parental magma ALV1659-001 (PetDB Database) on segment H along the GSC are shown in Figure 8 and Figure 9. Figure 8 shows the graphs where the calculations were done at QFM=0 while Figure 9 shows that the calculations were done at QFM=+1. From the graphs, it is observed that the parental magma agrees more with the samples when the calculations were set to QFM=+1 than at QFM=0. The calculated lines for SiO_2, TiO_2, FeO, and Na_2O fit better with the natural glasses when the QFM buffer was shifted to +1, however the lines for Al_2O_3 and CaO remain unaffected. The results also suggest that the low pressure, 0.5 kbar, produces the best fit for most of the samples at this segment.

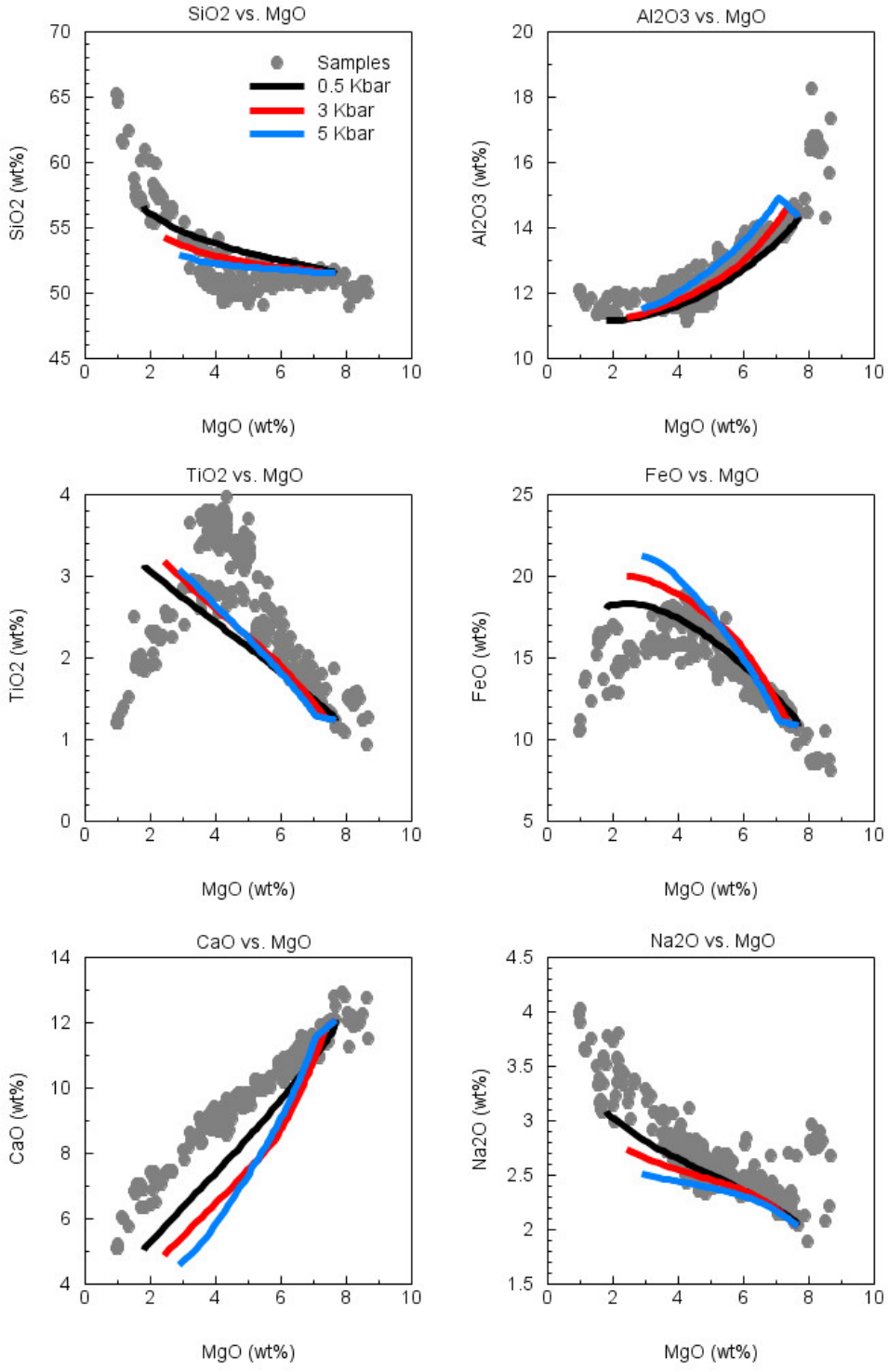

Figure 8: Graphs showing the weight % of the major oxides plotted against MgO for the parental magma ALV1659-001 (PetDB Database) on segment H along the GSC. The calculations were done using PETROLOG at various pressures (0.5 kbar, 3 kbar, and 5 kbar) and at a QFM buffer of 0.

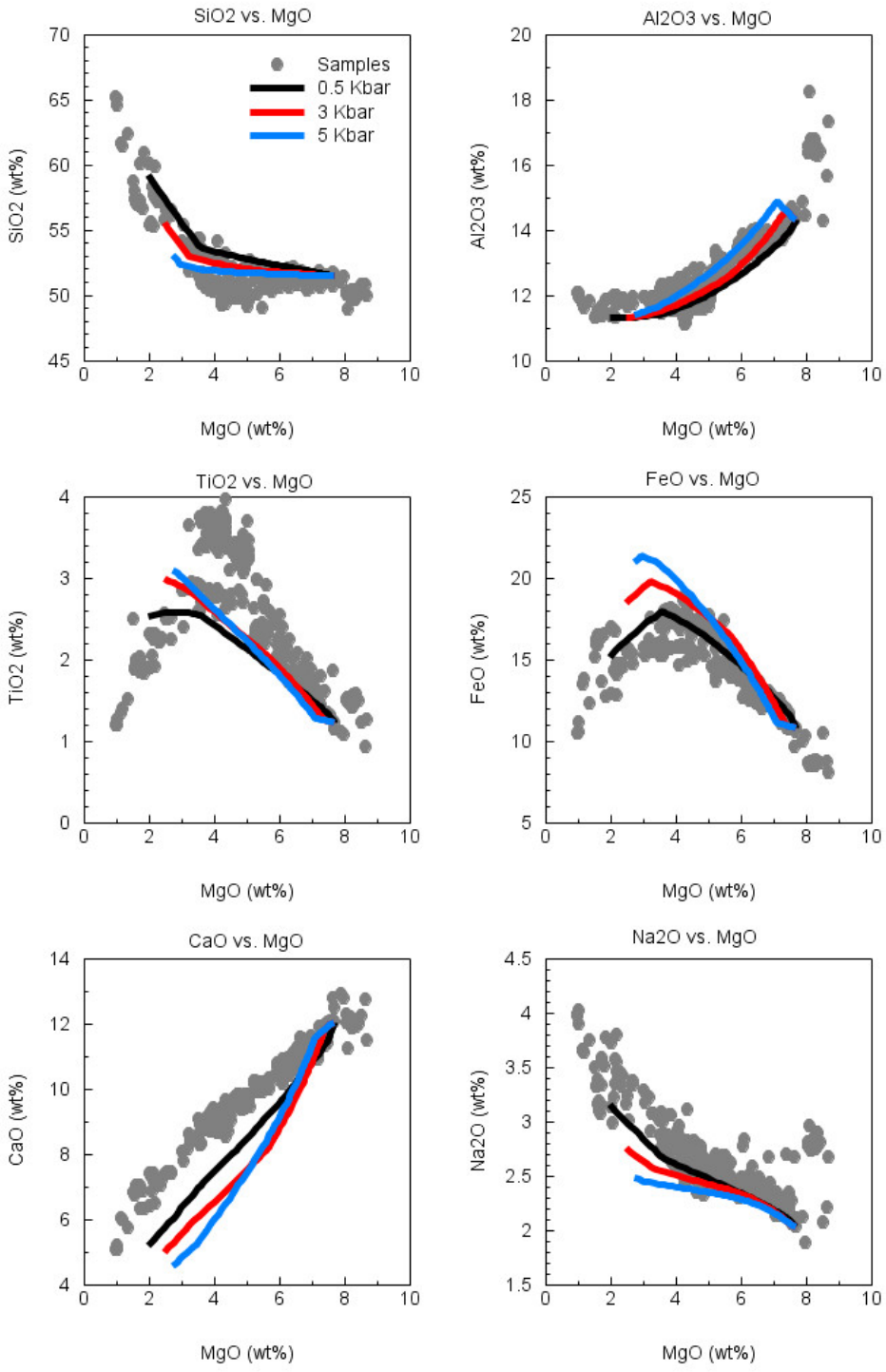

Figure 9: Graphs showing the weight % of the major oxides plotted against MgO for the parental magma ALV1659-001 (PetDB Database) on segment H along the GSC. The calculations were done using PETROLOG at various pressures (0.5 kbar, 3 kbar, and 5 kbar) and at a QFM buffer of +1.

DISCUSSION

Segment E exhibits a high MgO content ranging from 0.18 wt% to 9.69 wt% and the chosen parental magma, KAK1979-012-026 (PetDB Database) has a primitive parent composition (>8 wt% MgO). The samples conform best to the calculated liquids at low pressure, 0.5 kbar. The difference in crystallization pressure can have an implication on the crystallizing assemblages. This is evident in the plots of CaO against MgO (Figures 4 and 5), where the calculated lines for CaO at a high pressure, 5 kbar, decrease significantly as MgO decrease. In contrast, the parental magma shows an increase in CaO before it decreases again with decreasing MgO at a low pressure, 0.5 kbar, and this is due to the crystallization of olivine alone. However, the positive trends of CaO against MgO are consistent with the crystallization of clinopyroxene, olivine, and plagioclase. The plots of FeO and TiO in Figure 5 also indicate that the oxides fractionated from the magmas with less than ~4.5 wt% MgO. In Figure 3, it is shown that the melt is more enriched in P_2O_5 than K_2O as crystallization proceeds, which indicates that processes other than fractional crystallization have occurred in the segment. This is because the ratios of highly incompatible elements like P and K should have changed only a little in response to the process of crystallization (Macdougall, 1988) and yet, this segment shows a high ratio of P_2O_5/K_2O. Mixing by the process of assimilation during magma storage could possibly occur in this segment besides crystallization and explains the high P_2O_5/K_2O ratio.

The MORB primary magmas generally contain a small amount of water in the range of ~0.03–0.2 wt% (Danyushevsky, 2001). Addition of a small amount of water (0.1 wt%) to the starting composition reproduces the data better and this is because adding water will decrease the melt liquidus temperature and suppress plagioclase crystallization relative to olivine and clinopyroxene (Danyushevsky, 2001). This can be seen from Figure 5, where the calculated results for SiO_2, Al_2O_3, TiO_2, and FeO agree more with the natural samples when 0.1% water was added, whereas the calculated results for CaO and Na_2O are less affected by the addition of water. The smaller degree of plagioclase crystallization during cooling results in a higher Al_2O_3 wt% and a lower FeO wt% compared to the anhydrous crystallization (Figure 4). In fact, it is observed that there is a negative correlation between Al_2O_3 and FeO contents and this correlation is consistent with different extent of melting (Gale *et al.,* 2014).

Samples from segment F have a high content of TiO_2, Al_2O_3, Na_2O, and P_2O_5 and a low content of SiO_2, FeO, and CaO and these observations define segment F to be the location of the greatest plume influence along the GSC. The parental magma EWI0004-015-004 (Cushman, 2004) has a MgO content of ~8 wt% while the parental magma EWI0004-040-004 (Cushman, 2004) has a MgO content of >8 wt%. Crystallization at a low pressure, 0.5 kbar produces the most consistent fits of the calculated crystallization lines with the samples taken for both parents. However, the parental magma with ~8 wt% MgO composition agrees better with majority of the samples (Figure 6). The calculated crystallization results for TiO_2 for the parent EWI0004-040-004 (Cushman, 2004) are lower than the natural samples and its calculated crystallization lines for FeO are higher than the natural samples (Figure 7). This indicates that a primitive magma composition does not necessarily yield the best calculated crystallization lines for the samples when it comes to modeling the fractional crystallization of MORB. This segment, being in close proximity with the hotspot, exhibits greater and more variable degrees of fractionation. The relationship between P_2O_5 and K_2O in this segment shows increasing enrichment of incompatible elements, P and K, as

crystallization proceeds (Figure 3). This suggests that fractional crystallization was accompanied by other processes, such as mixing of varying amounts of depleted and enriched mantle end-members (Colman *et al.,* 2016). The high values of Na_8 in this segment are consistent with the occurrence of a low degree melting of a colder mantle (Figure D1).

The implications of shifting oxygen fugacity fO_2 values when performing calculations were explored on all segments, such that one calculation was set to QFM=0 and another was set to QFM=+1, where QFM is the quartz-fayalite-magnetite buffer. Previous work has suggested that even small changes in fO_2 can drastically affect the crystallization path (Peterman, 2017). The changes in fO_2 will change the oxidation state of Fe and this will be reflected in the mineral assemblages during crystallization (Peterman, 2017). This is apparent for Segment H in Figures 8 and 9, where the calculated crystallization lines for the parent ALV1659-001 (PetDB Database) with QFM=+1 fit better with the natural samples compared with the parent with QFM=0. SiO_2, TiO_2, and FeO are largely affected by the change in fO_2, whereas Al_2O_3, Na_2O, and CaO are less affected. It is also worth noting that the chemistry of the natural samples shown in Figure 8 is consistent with the crystallization of olivine, plagioclase, and clinopyroxene. However, the calculated crystallization lines for the selected parents in Segments E and F fit better when the calculations were set to QFM=0 instead of QFM=+1 (see Appendix A and Appendix B). For Segment H, the calculated crystallization lines for the parent ALV1659-001 (PetDB Database) with no water added to the initial melt agree more with the natural glasses as compared to the parent with 0.1% added water (see Appendix C). Once again, crystallization at low pressure, 0.5 kbar, best explains the composition of the natural samples in Segment H. Crustal assimilation may have also occurred in addition to crystallization in Segment H since the enrichment of P_2O_5 is more than K_2O in the melt as crystallization proceeds, resulting in the P_2O_5/K_2O ratio to be elevated (Figure 3). The low values of Na_8 in Segment H suggest that the magmas were produced by higher degrees of melting, signifying a hotter mantle (Figure D1).

The modeling of fractional crystallization of MORB along GSC using PETROLOG can be compared with the previous work done from Peterson *et al*. (2014). Addition of a small amount of water to the parental magma can have a large effect in the crystallization trends. This is shown in Figure 10, where the calculated crystallization trend lines for the samples taken near the Galápagos plume are different when 0.1% and 0.4% of water are added to the initial melt. This is consistent with the results found in this thesis, where a parental magma with different amount of water contents will produce different crystallization trend lines from the calculations done in PETROLOG.

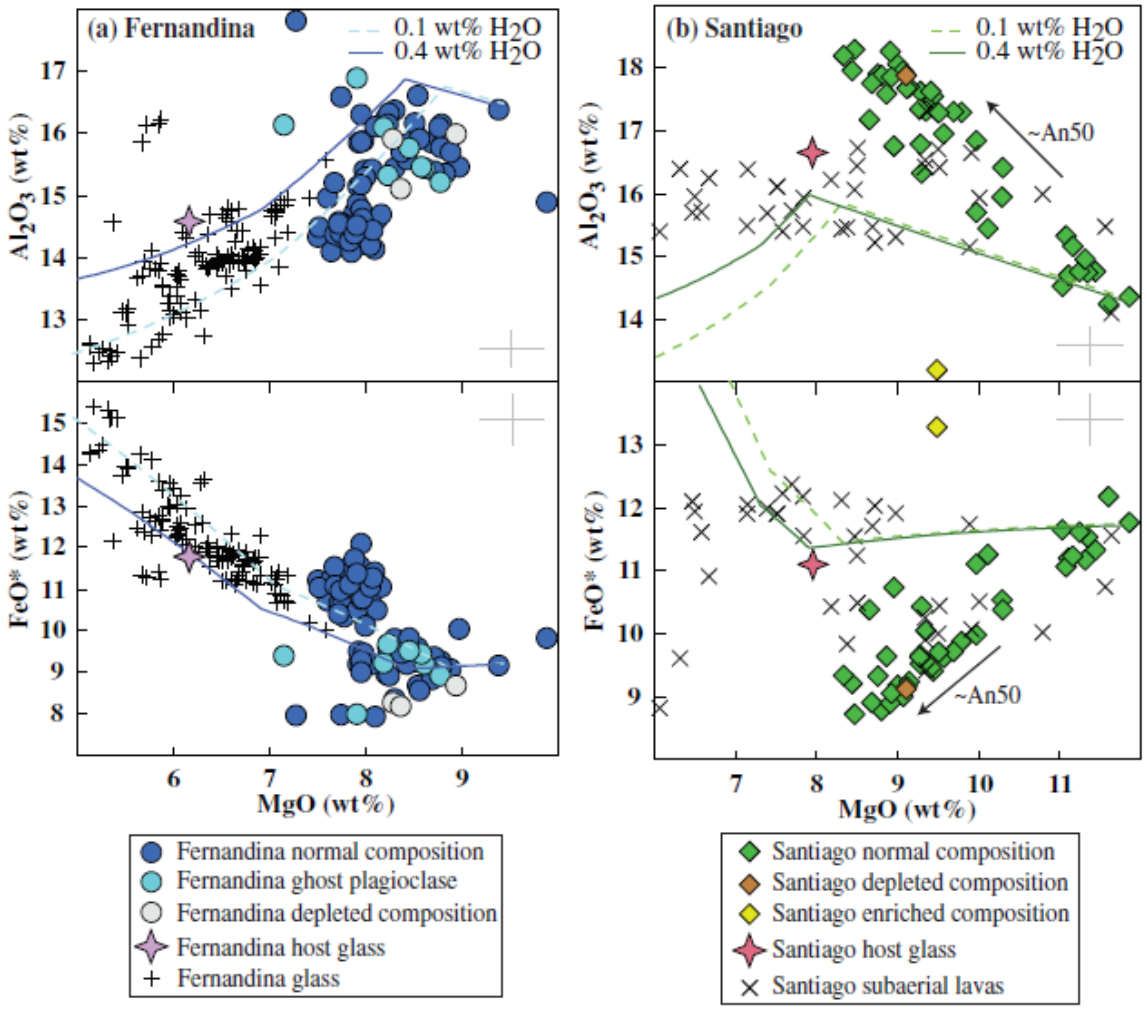

Figure 10: Variation of Al_2O_3 and FeO vs MgO wt%. Crystal fractionation trends were calculated using PETROLOG (Danyushevsky, 2001; Danyushevsky & Plechov, 2011) for Santiago and Fernandina melt inclusions at a pressure of 1.5 kbar for two concentrations of water: dashed line, 0.1 wt%; continuous line, 0.4 wt% water. Figure from Peterson *et al.* (2014).

The pressures of crystallization of MORB along the GSC have also been reported in previous work done in Haines (2016). It is observed that the pressure that best explain the composition of MORB in all three segments, 0.5 kbar, falls in the range of pressure stated in Haines (2016), which can be seen in Table 1. However, the average pressure for segment E and segment F are a little higher (~2 kbar) and this may be due to the difference in the number of samples taken.

Table 1: Table showing the ranges of pressure (in MPa), the average pressure (in MPa), and the number of samples for every segment. Table from Haines (2016).

Segment	Color	n_1	Range of P (MPa)	Average P (MPa)
A	Pink	58	.01-406.7	181.2
B	Yellow	10	16.2-941.7	500.8
C	Black	71	.01-917.3	338.42
D	Grey	91	.01-835.6	282.3
E	Blue	202	.01-517.76	251.8
F	Green	96	.01-695.4	225
G	White	3	36.4-462.1	298.3
H	Red	2	42.8-50.8	46.85
I	Navy	1	152.5	152.5
J	Orange	226	.01-779.6	389.9
K	Purple	16	.01-426.2	200.7
L	Cyan	14	48.3-360.9	258.1

CONCLUSIONS

The results presented in this thesis suggest that the lavas erupted along the Galápagos Spreading Center (GSC) went through multiple processes of magma evolution and vary in chemical compositions. The chemical compositions of all 1,777 analyzed glasses from three segments: E, F, and H can best be explained by modeling the fractional crystallization of mid-ocean ridge basalts (MORB) at a low pressure (0.5 kbar). The estimated pressure of partial crystallization of the minerals olivine, plagioclase, clinopyroxene, ilmenite, and magnetite present in basalts allows the depth in which the crystallization occurs to be determined. The amount of water content and oxygen fugacity of the parental magma also affect the degree of fractionation. It is observed that the calculated crystallization lines agree more to the natural samples when a small amount of water was added to the initial melt and the oxygen fugacity was shifted. Adding a small amount of water into the parental magma will suppress the crystallization of plagioclase relative to olivine and clinopyroxene while a shift in the oxygen fugacity will change the oxidation state of Fe which will be reflected in the mineral assemblages during crystallization. The work done in this thesis has also shown that a primitive magma composition does not necessarily produce the best calculated crystallization lines for the natural glasses on GSC. Analysis of P_2O_5 and K_2O contents provides evidence of crustal assimilation and mixing in addition to fractional crystallization. Elevated ratios of P_2O_5 and K_2O suggests that it was not possible for crystallization alone to make up the compositions of the samples taken along the GSC. Samples from segment F, which are strongly influenced by the mantle plume, contain high values of Na_8, which represents the occurrence of lower degree melting, while the low values of Na_8 from segments E and H are consistent with a higher degree of melting.

RECOMMENDATIONS FOR FUTURE WORK

Further analysis on the compositions of the erupted lavas needs to be done to elucidate the processes that accompanied the crystallization of the mid-ocean ridge magmas along the Galápagos Spreading Center (GSC). Future work should also include examining the rock samples taken from the area of interest in thin sections. The texture and mineral assemblages of the rock samples are useful in describing the physical and chemical conditions in which the rock forms. The findings on the recommended future work will further strengthen the evidence of mixing and crustal assimilation present during the magma evolution along the GSC. Future work should also include an additional study on the isotopic compositions since the isotopic compositions can also vary with the compositions of basalts.

REFERENCES CITED

Ariskin, A.A., and Barmina, G.S., 1999, An empirical model for the calculation of spinel-melt equilibria in mafic igneous systems at atmospheric pressure: 2. Fe-Ti oxides, Contrib. Mineral. Petrol., v. 134, p. 251–263, doi:10.1007/s004100050482.

Canales, J.P., Ito, G., Detrick, R. S., and Sinton, J., 2002, Crustal thickness along the western Galápagos Spreading Center and the compensation of the Galápagos hotspot swell: Earth and Planetary Science Letters, v. 203, p. 311-327.

Colman, A., Sinton, J.M., White, S.M., McClinton, J.T., Bowles, J.A., Rubin, K.H., Behn, M.D., Cushman, B., Eason, D.E., Gregg, T.K., Gronvold, K., Hidalgo, S., Howel.., J., Neill, O., and Russo, C., 2012, Effects of variable magma supply on mid-ocean ridge eruptions: Constraints from mapped lava flow fields along the Galápagos Spreading Center: Geochemistry, Geophysics, Geosystems, v. 13, no. 8, doi:10.1029/2012GC004163.

Colman, A., Sinton, J.M., and Rubin, K.H., 2016, Magmatic processes at variable magma supply along the Galápagos Spreading Center: Constraints from single eruptive units: Journal of Petrology, v. 57, no. 5, p. 981-1018, doi:10.1093/petrology/egw032.

Cushman, B., Sinton, J., Ito, G., and Dixon, J.E., 2004, Glass compositions, plume-ridge interaction, and hydrous melting along the Galápagos Spreading Center, 90.5°W to 98°W: Geochemistry, Geophysics, Geosystems, v. 5, no. 8. doi:10.1029/2004GC000709.

Crisp, J.A., 1984, Rates of magma emplacement and volcanic output: Journal of Volcanology and Geothermal Research, v. 20, p. 177-211.

Danyushevsky, L.V., 2001, The effect of small amounts of H_2O on crystallization of mid-ocean ridge and backarc basin magmas: Journal of Volcanology and Geothermal Research, v. 110, p. 265-280.

Danyushevsky, L.V., and Plechov P., 2011, Petrolog3: Integrated software for modeling crystallization processes: Geochemistry, Geophysics, Geosystems, v. 12, no. 7, doi:10.1029/2011GC003516.

Gale, A., Dalton, C.A., Langmuir, C.H., Su, Y., and Schilling, J., 2013, The mean composition of ocean ridge basalts: Geochemistry, Geophysics, Geosystems, v. 14, p. 489-518, doi:10.1029/2012GC004334.

Gale, A., Langmuir, C H., and Dalton, C A., 2014, The global systematics of ocean ridge basalts and their origin: Journal of Petrology, v. 55, no. 6, p. 1051-1082, doi:10.1093/petrology/egu017.

Gale, A., Laubier, M., Escrig, S., and Langmuir, C.H., 2013, Constraints on melting processes and plume-ridge interaction from comprehensive study of the FAMOUS and North Famous segments, Mid-Atlantic Ridge: Earth and Planetary Science Letters, v. 365, p. 209-220.

Giordano, D., and Dingwell, D. B., 2003, The kinetic fragility of natural silicate melts. Journal of Physics: Condensed Matter, v. 15, p. S945.

Haines, K.A., 2016, The pressures of partial crystallization along the Galápagos spreading center, B.S. Thesis, p. 24. https://kb.osu.edu/bitstream/handle/1811/86236/Katherine_Haines_Thesis.pdf?sequence=1&isAllowed=y.

Herbrich, A., Hauff, F., Hoernle, K., Werner, R., Garbe-Schönberg, D., and White, S., 2016, A 1.5 Ma record of plume-ridge interaction at the Western Galápagos Spreading Center (91°40'–92°00'W): Geochimica Et Cosmochimica Acta, v. 185, p. 141-159, doi: 10.1016/j.gca.2016.04.036.

Kokfelt, T.F., Lundstrom, C., Hoernle, K., Hauff, F., and Werner, R., 2005, Plume-ridge interaction studied at the Galápagos spreading center: Evidence from ^{226}Ra-^{230}Th-^{238}U and ^{231}Pa-^{235}U isotopic disequilibria: Earth and Planetary Science Letters, v. 234, p. 165-187, doi:10.1016/j.epsl.2005.02.031.

Kress, V.C., and Carmichael, I.S.E., 1988, Stoichiometry of the iron oxidation reaction in silicate melts: American Mineralogist, v. 73, p. 1267-1274.

Lange, R.A. and Carmichael, I.S.E., 1987, Densities of Na2O-K2O-CaO-MgO-FeO-Fe2O3-Al2O3-TiO2-SiO2 liquids: new measurements and derived partial molar properties: Geochimica et Cosmochimica Acta, v. 51, p. 2931-2946.

Langmuir, C. H., Klein, E.M., and Plank, T., 1992, Petrological systematics of mid-ocean ridge basalts: Constraints on melt generation beneath ocean ridges: Mantle Flow and Melt Generation at Mid-Ocean Ridges Geophysical Monograph Series v. 71, p.183-280.

Macdonald, K.C., 2001, Mid-ocean Ridge Tectonics, Volcanism, and Geomorphology: Encyclopedia of Ocean Sciences, p. 1798-1813, doi:10.1006/rwos.2001.0094.

Macdougall, J.D., 1988, Continental Flood Basalts: Petrology and Structural Geology, Kluwer Academic Publishers, p. 341.

Merlen, G., 2014, Plate tectonics, evolution, and the survival of species: Geophysical Monograph Series, doi:10.1002/9781118852538.ch7.

Niu, Y.L. and Batiza, R., 1994, Magmatic processes at a slow spreading ridge segment: 26°S Mid-Atlantic Ridge: Journal of Geophysicial Research: Solid Earth, v. 99, p. 19719-19740, doi:10.1029/94JB01663

O'Hara, M.J., 1977, Geochemical evolution during fractional crystallization of a periodically refilled magma chamber: Nature, v. 266, p. 503-507.

O'Hara, M.J., 1985, Importance of the "shape" of the melting regime during partial melting of the mantle: Nature, v. 314, p. 58-62.

PetDB Database: www.earthchem.org/petdb (accessed March 2018).

Peterman, K.J., 2017, Determination of Oxygen Fugacity using Olivine-Melt Equilibrium: Implications for the Redox States of Mid-Ocean Ridge Basalt and Ocean Island Basalt Mantle Source Regions, p. 98.

Peterson, M.E., Saal, A.E., Nakamura, E., Kitagawa, H., Kurz, M.D., and Koleszar, A.M., 2014, Origin of the 'ghost plagioclase' signature in Galápagos melt inclusions: New evidence

from Pb isotopes: Journal of Petrology, v. 55, no. 11, p. 2193-2216, doi:10.1093/petrology/egu054.

APPENDIX A

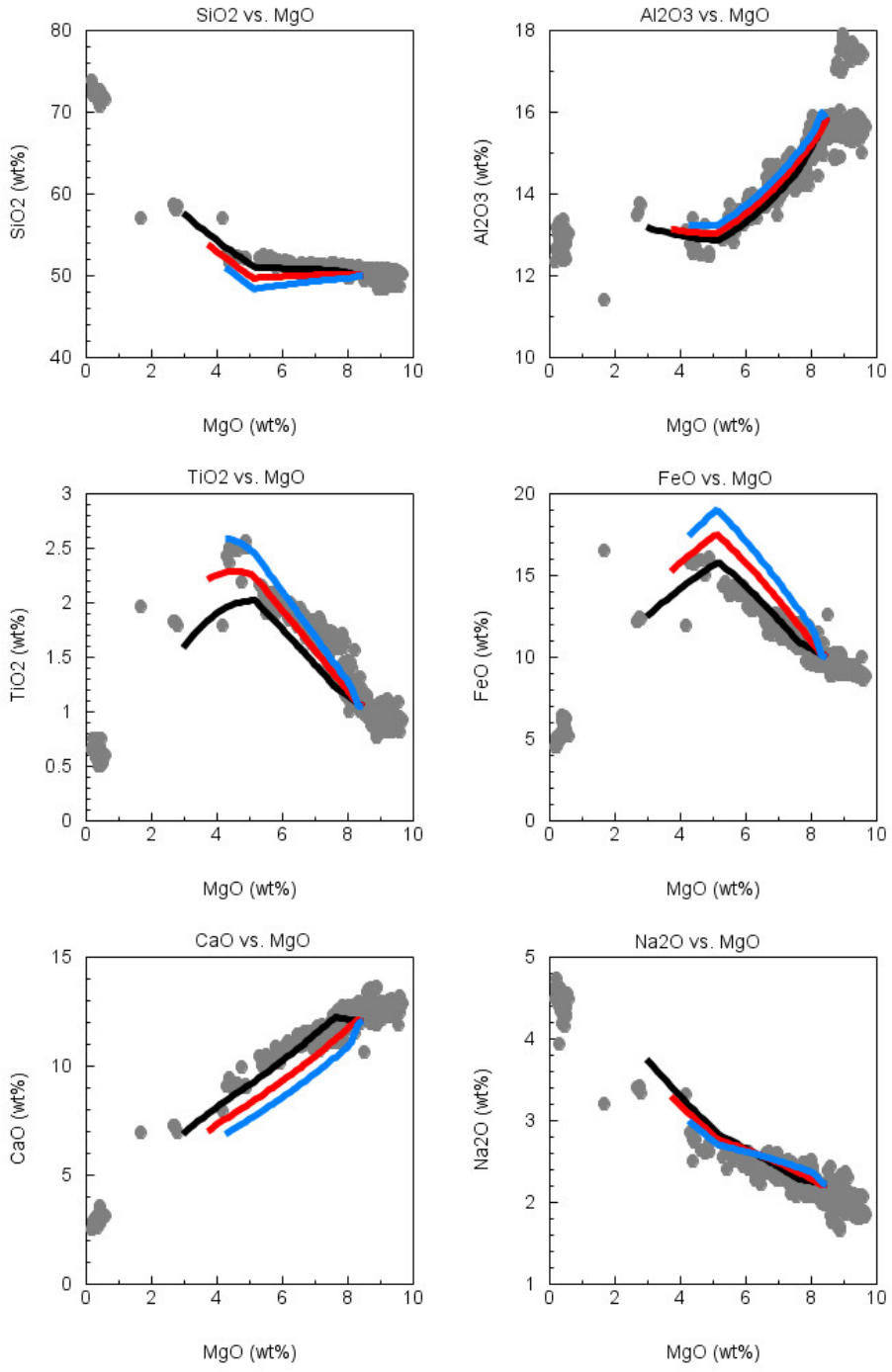

Figure A1: Graphs showing the weight % of the major oxides plotted against MgO for the parental magma KAK1979-012-026 (PetDB Database) on segment E along the GSC. The calculations were done using PETROLOG at various pressures (0.5 kbar, 3 kbar, and 5 kbar) with 0.1% water added to the initial melt and at a QFM buffer of +1.

APPENDIX B

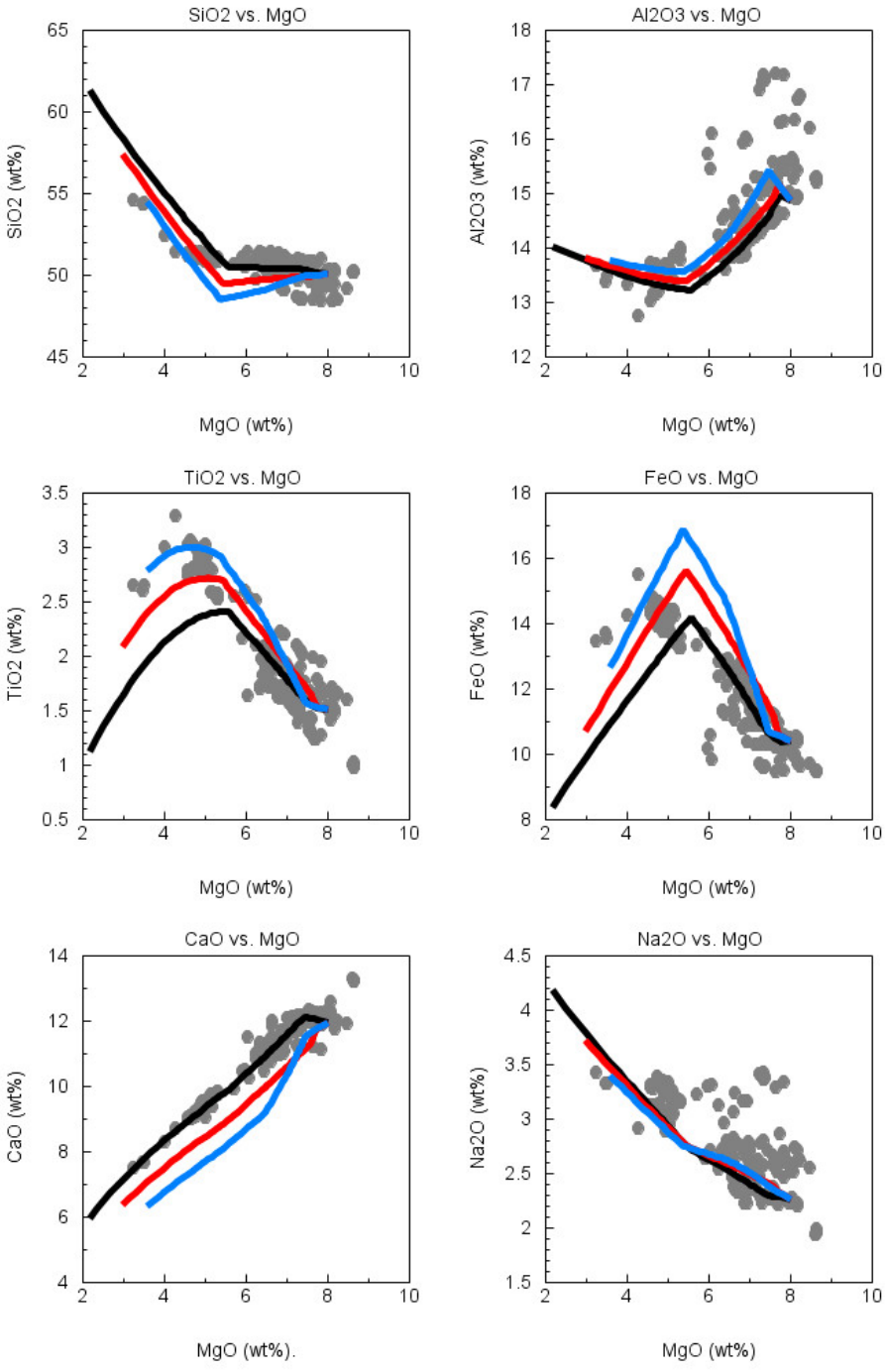

Figure B1: Graphs showing the weight % of the major oxides plotted against MgO for the parental magma EWI0004-015-004 (Cushman et al., 2004) on segment F along the GSC. The calculations were done using PETROLOG at various pressures (0.5 kbar, 3 kbar, and 5 kbar) with 0.2% water added to the initial melt and at a QFM buffer of +1.

APPENDIX C

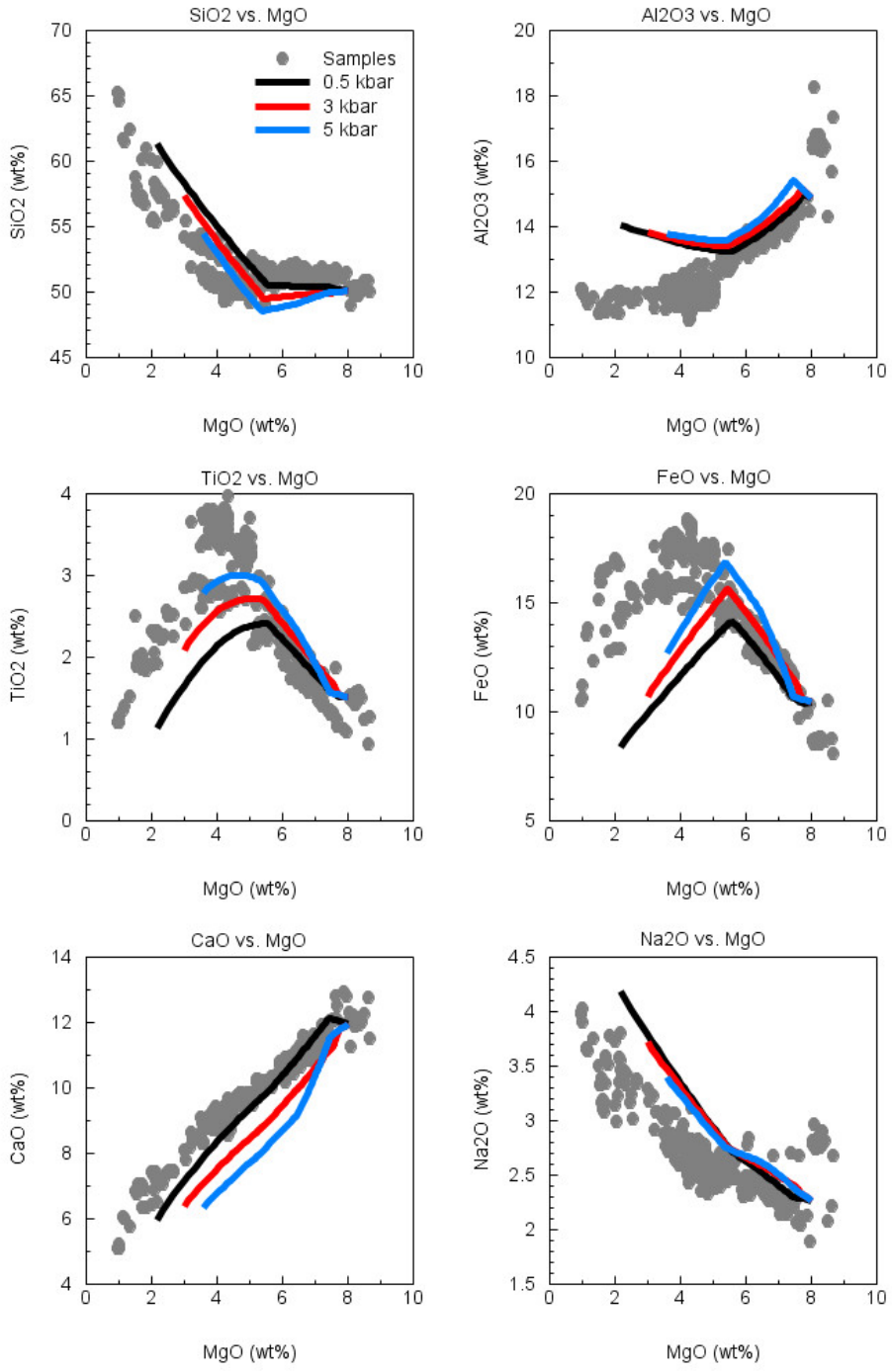

Figure C1: Graphs showing the weight % of the major oxides plotted against MgO for the parental magma ALV1659-001 (PetDB Database) on segment H along the GSC. The calculations were done using PETROLOG at various pressures (0.5 kbar, 3 kbar, and 5 kbar) with 0.1% water added to the initial melt and at a QFM buffer of +1.

APPENDIX D

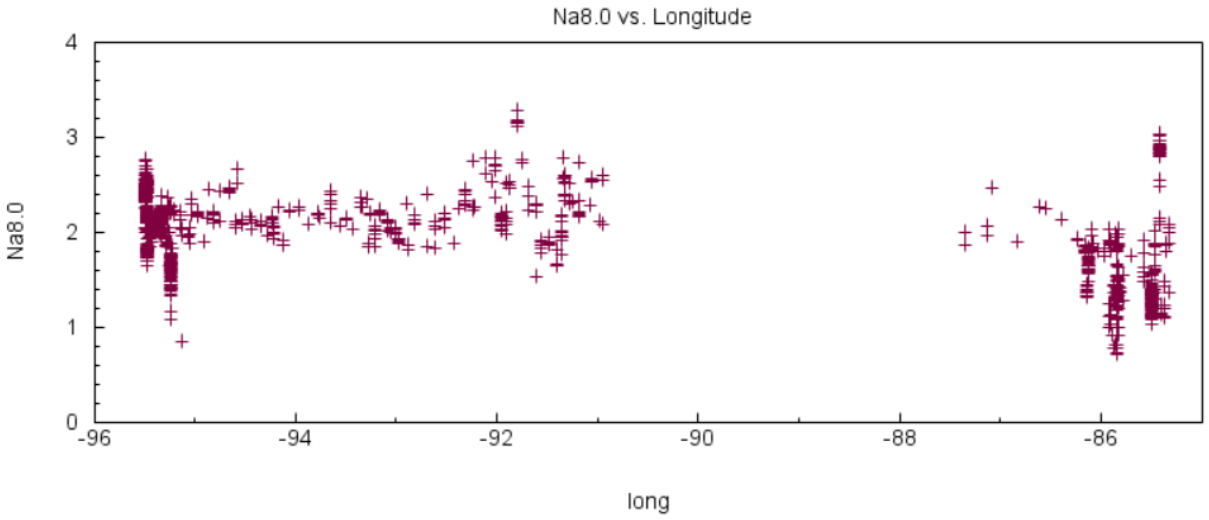

Figure D1: Plot of corrected Na values, Na_8 against longitude of segments E, F, and H.

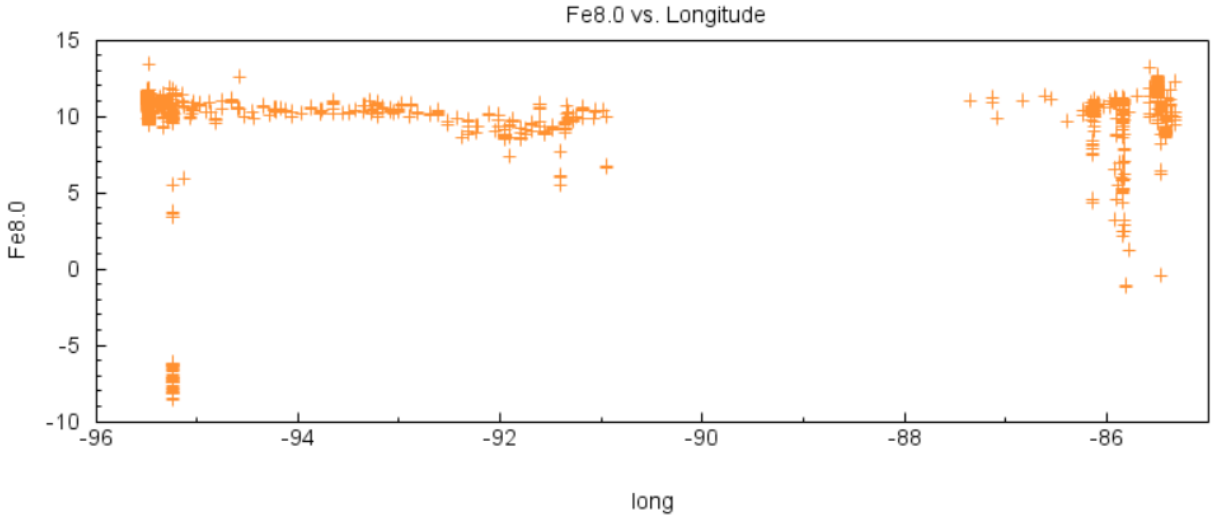

Figure D2: Plot of corrected Fe values, Fe_8 against longitude of segments E, F, and H.

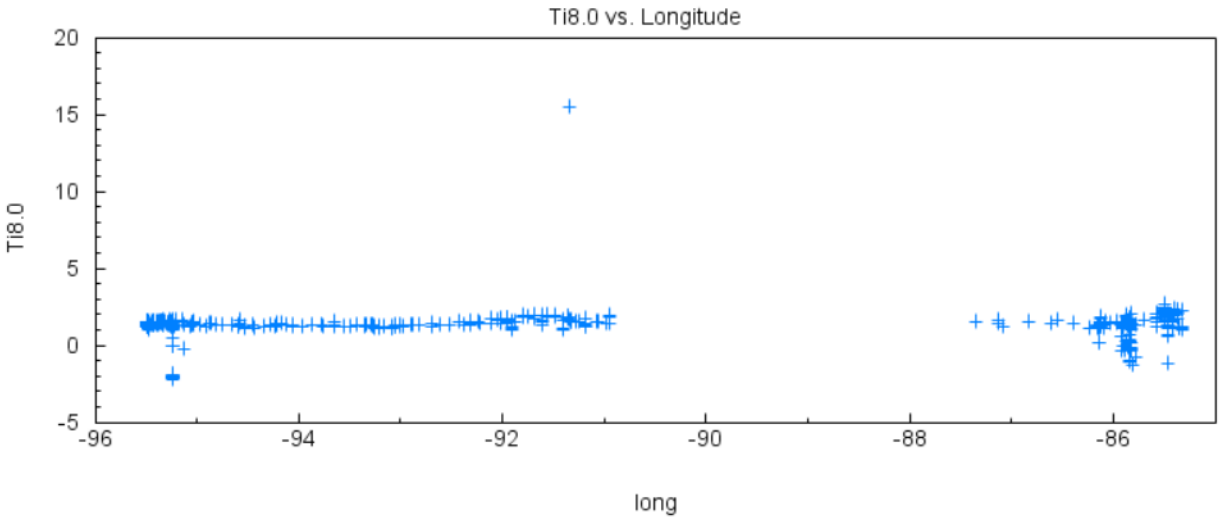

Figure D3: Plot of corrected Ti value, Ti_8 against longitude of segments E, F, and H.

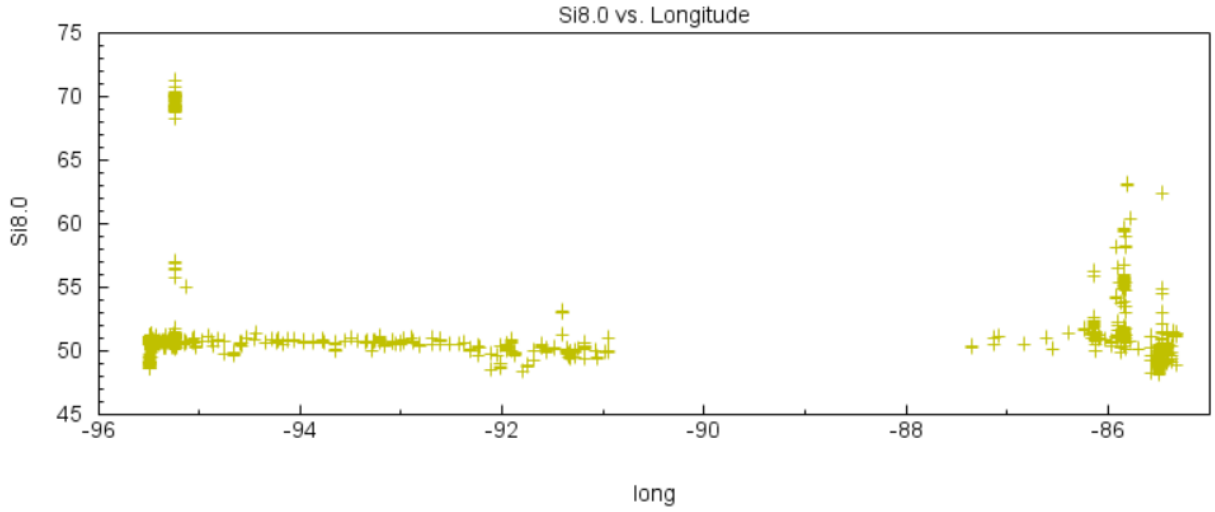

Figure D4: Plot of corrected Si values, Si_8 against longitude of segments E, F, and H.